American Mineralogist, Volume 89, pages 932–940, 2004

Structural variations induced by difference of the inert pair effect in the stibnite-bismuthinite solid solution series $(Sb,Bi)_2S_3$

ATSUSHI KYONO[1,*] AND MITSUYOSHI KIMATA[2]

[1]Laboratory for Entrepreneurship, University of Tsukuba, Tennodai 1-1-1, Tsukuba, Ibaraki, 305-8573, Japan
[2]Institute of Geoscience, University of Tsukuba, Tennodai 1-1-1, Tsukuba, Ibaraki, 305-8571, Japan

ABSTRACT

Structural refinements of single crystal X-ray diffraction data for synthetic $(Sb,Bi)_2S_3$ solid solutions revealed structural variations in the stibnite (Sb_2S_3)-bismuthinite (Bi_2S_3) series. Coordination environments of the M cations are (3 + 4)-fold for the M1 site and (5 + 2)-fold for the M2 site. For the M1 and M2 polyhedra, the short M-S bond lengths increase constantly with increasing Bi concentration, whereas the long M-S bond lengths decrease continuously. The S-M-S interatomic angles interposing lone-pair electrons increase continuously from stibnite to bismuthinite. Stereochemical activity of the lone-pair electrons induces configurational changes of ligands around the M cations from elongated ellipsoidal coordinations to spheroidal ones. Substitution of Bi^{3+} for Sb^{3+} in the solid solution expands the basic building block, which causes linear increase of the *b* lattice parameter with slight positive deviation from Vegard's law. This feature is ascribed to order-disorder with concentration of Sb at the M1 site and Bi at the smaller M2 site. Furthermore, increased Bi content engenders both expansion of the basic building block and contraction of intervals between these blocks, contributing to smaller changes in the *a* and *c* lattice parameters than in the *b* lattice parameter. The M2 polyhedra expand relative to the M1 polyhedra with increasing Bi content because the large Bi cation is concentrated at the smaller M2 site. One striking characteristic of $(Sb,Bi)_2S_3$ crystal structures is that geometries of central M cation and ligand atoms can be adapted flexibly to transformation of stereochemical activity from $5s^2$ lone-pair electrons to Bi $6s^2$ lone-pair electrons by altering the centroid-central atom distance and by changing angles of the centroid-central atom to the *a* axis.

INTRODUCTION

The minerals bismuthinite (Bi_2S_3) and stibnite (Sb_2S_3) have identical crystal structures; volumes of their orthorhombic unit cells differ by 3.5% at most (Springer and Laflamme 1971). These crystal structures have been studied by several authors (Bayliss and Nowacki 1972; Kanishcheva et al. 1981; Łukaszewicz et al. 1999; Kyono et al. 2002; Lundegaard et al. 2003). The solid solution between the two phases has been investigated through chemical analyses (Springer 1969; Springer and Laflamme 1971; Nayak et al. 1983). In hydrothermal ore deposits, the bismuthinite-stibnite series exhibits distinct compositional variations along flow paths of mineralizing fluids in ore deposits (Springer 1969; Lueth et al. 1990) that are characterized by preponderance of mole Bi/(Sb + Bi) ratios near the end-members. There is a conspicuous paucity of intermediate compositions (Ghosal and Sack 1999). Lueth et al. (1990) attributed such variations in Bi/(Sb + Bi) molar ratios to a process referred to as "semi-metal boiling," whereby preferential volatilization of antimony from the ore fluid at a point along the flow path is inferred to cause sudden change in the stibnite-bismuthinite Sb/Bi ratio. However, interpretation of this solid solution has been restricted to unit-cell parameters calculated from X-ray powder diffraction data (e.g., Nayak et al. 1983) because structural refinements have not been performed on the $(Sb,Bi)_2S_3$ solid solution. Concerning lone-pair electrons, the differences in stereochemical activity between Sb and Bi cations has been described in detail from crystal structure data (Makovicky 1981, 1992; Pfitzner and Kurowski 2000). A recent single-crystal X-ray diffraction study documented that a phase transition in a stibiocolumbite-bismutocolumbite solid solution is caused by differential stereochemical activity (Kazantsev et al. 2002). A variety of stereochemical activities (inert pair effects) induced by Sb $5s^2$ and Bi $6s^2$ lone-pair electrons affect structural modification directly because stibnite and bismuthinite are composed entirely of coordinated polyhedra enclosing stereoactive lone-pair electrons.

The present study specifically addresses the effect on the crystal structure of substitution of Bi^{3+} for Sb^{3+} in the $(Sb,Bi)_2S_3$ solid solution series, focusing on the shift and dynamics of stereochemical activity from Sb $5s^2$ to Bi $6s^2$ lone-pair electrons.

EXPERIMENTAL METHODS

Sample preparation

Samples of stibnite and bismuthinite were selected from specimens from an antimony mine in Xikuangshan, China, and from the Gabriel Vein, Tafna, Bolivia, respectively. The samples and their purity were verified by electron microprobe and X-ray diffraction analyses (Table 1). Both stibnite and bismuthinite exhibited ideal chemical compositions; Ag, Fe, Cu, Zn, Sn, Pb, Tl, Se, and Te were sought but not detected. The methods of synthesis were similar to those described by Springer and Laflamme (1971), except for temperatures. The stibnite and bismuthinite used as starting materials were carefully extracted and mixed in an agate mortar according to their molar ratios listed in Table 2. Finely powdered samples were put into quartz ampoules, which were evacuated and sealed. The ampoules were then heated in an electronic furnace (Table 2). After the reaction, the ampoules were taken out of the furnace and quenched in air at room temperature. Single crystals obtained

* E-mail: kyono@arsia.geo.tsukuba.ac.jp

TABLE 1. Crystallographic data for structure determination of stibnite (Sb_2S_3), bismuthinite (Bi_2S_3), and synthetic $(Sb,Bi)_2S_3$

Chemical composition	**$Sb_{2.000}S_3$(1)**	**$Sb_{2.000}S_3$(2)**	**$Sb_{2.000}S_3$(3)**	**$Sb_{2.000}S_3$(4)**	**$Sb_{1.935}Bi_{0.065}S_3$**
Crystal system	Orthorhombic	Orthorhombic	Orthorhombic	Orthorhombic	Orthorhombic
Space group	*Pnma*	*Pnma*	*Pnma*	*Pnma*	*Pnma*
Crystal size (mm)	0.40 × 0.30 × 0.10	0.40 × 0.10 × 0.10	0.40 × 0.40 × 0.10	0.80 × 0.10 × 0.10	0.60 × 0.10 × 0.10
Z	4	4	4	4	4
a (Å)	11.282(3)	11.311(1)	11.2845(8)	11.3197(9)	11.3122(9)
b (Å)	3.8296(7)	3.8389(3)	3.8220(3)	3.8332(2)	3.8428(2)
c (Å)	11.225(2)	11.223(1)	11.203(2)	11.2330(8)	11.221(1)
V (Å^3)	485.0(2)	487.31(7)	483.16(8)	487.41(6)	487.80(7)
Calc. density (g·cm^{-3})	4.652	4.630	4.669	4.629	4.696
F(000)	600.00	600.00	600.00	600.00	607.69
Absorption coefficient (cm^{-1})	122.20	121.62	122.66	121.59	139.76
Exposure rate (s/°)	60	60	60	60	60
Maximum 2θ (°)	54.9	55.0	54.9	54.9	54.9
No. of measured reflections, R_{int}	3369, 0.041	3528, 0.059	3521, 0.073	4371, 0.030	4181, 0.037
No. of independent reflections	682	695	677	687	638
No. of observed reflections	597	560	537	597	571
No. of parameters	31	31	31	31	37
R, *Rw* for $F_o > 3$ (F_o)	0.031, 0.036	0.031, 0.035	0.036, 0.044	0.023, 0.025	0.022, 0.025
GooF	1.10	1.06	1.05	1.14	1.02
Difference map (e Å^{-3})	2.52	2.59	1.84	1.56	0.67
	−1.07	−1.74	−1.37	−0.86	−1.97

Chemical composition	**$Sb_{1.637}Bi_{0.363}S_3$**	**$Sb_{1.483}Bi_{0.517}S_3$**	**$Sb_{1.463}Bi_{0.537}S_3$**	**$Sb_{1.426}Bi_{0.574}S_3$**	**$Sb_{0.910}Bi_{1.090}S_3$**
Crystal system	Orthorhombic	Orthorhombic	Orthorhombic	Orthorhombic	Orthorhombic
Space group	*Pnma*	*Pnma*	*Pnma*	*Pnma*	*Pnma*
Crystal size (mm)	0.40 × 0.05 × 0.05	0.50 × 0.10 × 0.05	0.80 × 0.05 × 0.05	0.60 × 0.05 × 0.05	0.40 × 0.05 × 0.05
Z	4	4	4	4	4
a (Å)	11.274(3)	11.318(3)	11.309(1)	11.318(2)	11.256(2)
b (Å)	3.8739(8)	3.883(2)	3.871(2)	3.8872(4)	3.8966(5)
c (Å)	11.160(1)	11.226(5)	11.1876(3)	11.228(2)	11.205(2)
V (Å^3)	487.4(2)	493.4(3)	489.7(2)	494.0(1)	491.5(1)
Calc. density (g·cm^{-3})	5.056	5.185	5.246	5.235	5.875
F(000)	646.08	666.56	669.12	672.96	739.52
Absorption coefficient (cm^{-1})	231.23	276.57	284.71	291.26	449.81
Exposure rate (s/°)	60	90	120	180	60
Maximum 2θ (°)	55.0	54.9	54.9	55.0	54.9
No. of measured reflections, R_{int}	3332, 0.102	3153, 0.084	3628, 0.098	3461, 0.062	3052, 0.074
No. of independent reflections	638	1274	637	636	1745
No. of observed reflections	381	380	478	456	406
No. of parameters	37	37	37	37	37
R, *Rw* for $F_o > 3$ (F_o)	0.036, 0.039	0.049, 0.053	0.041, 0.049	0.032, 0.035	0.045, 0.048
GooF	1.05	1.12	1.11	1.07	1.13
Difference map (e Å^{-3})	1.60	2.01	1.52	2.57	3.05
	−1.57	−2.39	−2.51	−1.49	−2.88

Chemical composition	**$Sb_{0.387}Bi_{1.613}S_3$**	**$Sb_{0.362}Bi_{1.638}S_3$**	**$Sb_{0.320}Bi_{1.680}S_3$**	**$Bi_{2.000}S_3$(1)**	**$Bi_{2.000}S_3$(2)**
Crystal system	Orthorhombic	Orthorhombic	Orthorhombic	Orthorhombic	Orthorhombic
Space group	*Pnma*	*Pnma*	*Pnma*	*Pnma*	*Pnma*
Crystal size (mm)	0.50 × 0.05 × 0.05	0.80 × 0.05 × 0.05	1.2 × 0.05 × 0.05	0.60 × 0.05 × 0.05	0.30 × 0.05 × 0.05
Z	4	4	4	4	4
a (Å)	11.336(3)	11.310(1)	11.3180(4)	11.316(3)	11.345(3)
b (Å)	3.9562(7)	3.9526(4)	3.9547(2)	3.9709(2)	3.994(1)
c (Å)	11.186(3)	11.119(1)	11.1631(6)	11.178(2)	11.193(4)
V (Å^3)	501.7(2)	499.74(8)	499.64(4)	502.3(2)	507.2(2)
Calc. density (g·cm^{-3})	6.357	6.416	6.463	6.799	6.732
F(000)	806.08	809.92	815.04	856.00	856.00
Absorption coefficient (cm^{-1})	594.55	605.74	617.73	709.11	702.16
Exposure rate (s/°)	60	60	60	120	180
Maximum 2θ (°)	55.0	54.9	54.9	55.0	54.9
No. of measured reflections, R_{int}	3028, 0.051	3420, 0.054	4197, 0.038	3737, 0.094	3831, 0.087
No. of independent reflections	1009	2032	2188	1668	1720
No. of observed reflections	508	519	558	570	445
No. of parameters	37	37	37	31	31
R, *Rw* for $F_o > 3$ (F_o)	0.036, 0.048	0.026, 0.038	0.023, 0.025	0.049, 0.059	0.039, 0.046
GooF	1.05	1.03	1.12	1.02	1.06
Difference map (e Å^{-3})	2.75	2.23	1.84	4.13	2.90
	−2.29	−2.22	−2.43	−3.97	−3.32

through these syntheses attained a maximum size of 2.0 × 0.1 × 0.1 mm. Electron microprobe analyses were performed with a JEOL Superprobe (JXA-8621) operated at 25 kV and 10 nA sample current. The following standards were used for elements shown in parentheses: pyrite (S*K*α), stibnite (Sb*L*α), and Bi_2Te_3 (Bi*M*α). Table 2 summarizes the results of the quantitative analyses.

Structure solution and refinement

Single crystals from these experiments were selected for subsequent X-ray diffraction data collection. Micro-twinning in all single crystals was carefully examined by Laue spots on imaging plates. Data collection was conducted with an imaging plate diffractometer (Rigaku RAXIS-RAPID) using graphite monochro-

TABLE 1.—*continued*

Chemical composition	**$Bi_{2.000}S_3$(3)**
Crystal system	Orthorhombic
Space group	*Pnma*
Crystal size (mm)	0.50 × 0.05 × 0.05
Z	4
a (Å)	11.3540(4)
b (Å)	3.9911(1)
c (Å)	11.188(2)
V (Å^3)	507.01(9)
Calc. density (g·cm^{-3})	6.735
F(000)	856.00
Absorption coefficient (cm^{-1})	702.46
Exposure rate (s/°)	60
Maximum 2θ (°)	54.9
No. of measured reflections, R_{int}	3859, 0.107
No. of independent reflections	1414
No. of observed reflections	404
No. of parameters	31
R, *Rw* for $F_o > 3$ (F_o)	0.044, 0.049
GooF	1.09
Difference map (e Å^{-3})	2.53
	−3.86

mated Mo*K*α radiation (λ = 0.71069 Å). Measured intensities were corrected for Lorentz and polarization factors. The structure was resolved using direct methods with the program SIR92 (Altomare et al. 1992) and expanded using Fourier techniques with the program DIRDIF99 (Beurskens et al. 1999). Full-matrix least squares refinement was performed with the CRYSTALS program (Watkin et al. 1996). Reflections with $F_o > 3\sigma(F_o)$ were used for all refinements. Values of *R* ranged from 0.08 to 0.10 by this stage. After data collection, the chemical composition of each crystal was determined from averages of 6–10 points analyzed with the microprobe (Table 2). Crystals obtained through the synthesis experiments were found to be totally homogeneous by SEM-EDS analyses (Fig. 1). Empirical formulae were normalized on the basis of five atoms per formula unit. The ratio of Sb/Bi was considered to be equal to the measured Sb/Bi ratio (Table 2) based on the initial assumption that the M cations are disordered because the M sites (M = Sb, Bi) are fully occupied by trivalent cations alone. The *R*-values of subsequent structure models were improved to between *R* = 0.03–0.06. The assumption of a distorted Sb-Bi distribution was then relaxed. Table 1 summarizes structural data and details of structural refinement for all investigated samples. Table 3 contains fractional atomic coordinates and isotropic displacement parameters. Table 4 lists anisotropic displacement parameters.

RESULTS AND DISCUSSION

Lattice parameters

The functional relations between variations in unit cell parameters *a*, *b*, *c*, *V*, and Bi concentration are illustrated in Figure 2. Wide spreads are observed for both the *a* and *c* parameters. Although we performed a careful diffraction reinvestigation with a four-circle diffractometer as well, the variations in cell parameters are fairly similar to those observed by the IP diffractometer. Substitution of Bi^{3+} for Sb^{3+} predominantly influences the *b* lattice parameter, which increases linearly by 4.5%, as well as the unit cell volume *V*, which increases monotonically by 5.0%. Nayak et al. (1983) demonstrated that Vegard's law is obeyed over the whole range of Sb_2S_3-Bi_2S_3 solid solution. However, changes of *a* and *c* lattice parameters are distinctly non-linear (the plots show scattered data points throughout the range); even differences between the two end-member compositions can be almost negligible (Fig. 2). This can be regarded as one of the important features for the $(Sb,Bi)_2S_3$ solid solution series, and the changes in unit-cell volume mainly result from the linear increase of the *b* lattice parameter. Figure 2 shows that the solid solution exhibits slight positive deviation from linearity in variations of *b* and *V*

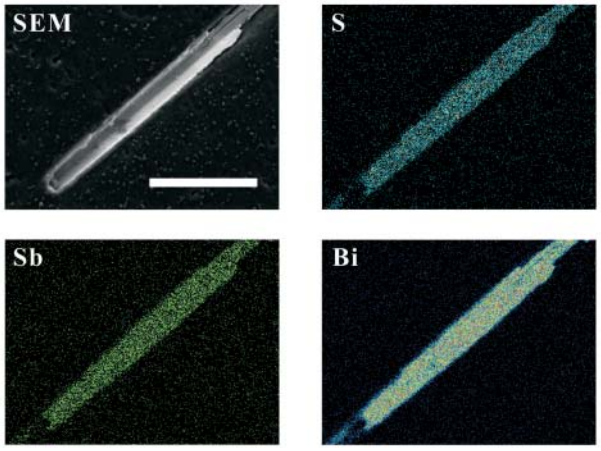

FIGURE 1. Secondary electron and X-ray element map images of polished surface of synthetic $(Sb,Bi)_2S_3$ prepared the with molar ratio stibnite:bismuthinite = 1:3. The sample displays chemical homogeneity throughout the crystal. The scale bar is 50 μm.

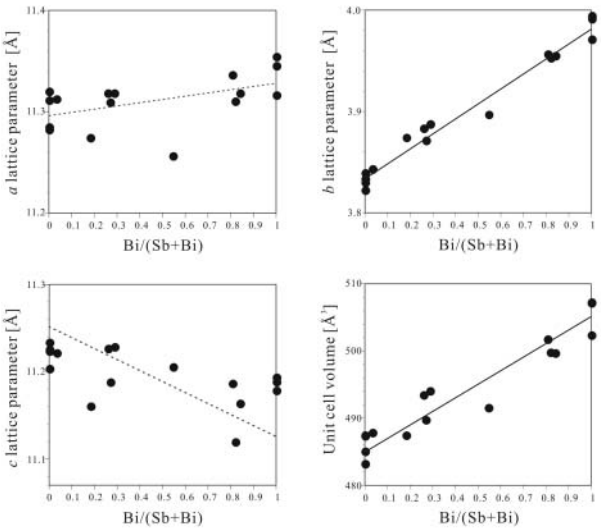

FIGURE 2. Lattice parameters of the synthetic stibnite-bismuthinite $(Sb,Bi)_2S_3$ solid solution series. The solid lines are linear least-square fits to the data with the coefficient of determination $R^2 > 90\%$**.** The dashed lines are fitted with the coefficient of determination $R^2 < 90\%$.

parameters. Although positive deviation of the *b* lattice parameter from Vegard's law is similar to experimental results interpreted as long-range order of cations in the solid solution (Toman 1978; Weinberger et al. 1994), anisotropic variations in lattice parameters, such as a significant increase in only the *b* axis, may be ascribed to anisotropy of Sb and Bi cations with stereoactive lone-pair electrons (Makovicky 1981, 1992; Pfitzner and Kurowski 2000).

The M1 site

The basic building block in crystal structures of bismuthinite-stibnite $(Sb,Bi)_2S_3$ solid solution series forms infinite $[M_4S_6]$ ribbons (Makovicky 1981) that run parallel to **b**. They are identical to those of stibnite described by Skowron and Brown (1994). Figure 3 shows variations of individual M1-S bond lengths in the $(Sb,Bi)_2S_3$ solid solution. As previously noted by Kyono et

TABLE 2. Synthetic conditions and the results of electron microprobe investigations for synthetic $(Sb,Bi)_2S_3$

Experiment no.	Molar ratio stibnite:bismuthinite	T (°C)	Time (d)	Products				
				Sb	Bi	S	Sb/Bi	Chemical composition
Sb4Bi1-1	4:1	650	8	1.884	0.063	3.054	0.968/0.032	$Sb_{1.935}Bi_{0.065}S_3$
Sb1Bi1-3	1:1	720	4	1.621	0.360	3.020	0.818/0.182	$Sb_{1.637}Bi_{0.363}S_3$
Sb1Bi1-7	1:1	720	4	1.473	0.513	3.014	0.742/0.258	$Sb_{1.483}Bi_{0.517}S_3$
Sb1Bi1-13	1:1	720	4	1.449	0.531	3.020	0.732/0.268	$Sb_{1.463}Bi_{0.537}S_3$
Sb1Bi1-12	1:1	720	4	1.413	0.569	3.018	0.713/0.287	$Sb_{1.426}Bi_{0.574}S_3$
Sb1Bi1-14	1:1	720	4	0.930	1.115	2.956	0.455/0.545	$Sb_{0.910}Bi_{1.090}S_3$
Sb1Bi3-5	1:3	800	3	0.390	1.625	2.985	0.194/0.806	$Sb_{0.387}Bi_{1.613}S_3$
Sb1Bi3-11	1:3	800	3	0.364	1.648	2.988	0.181/0.819	$Sb_{0.362}Bi_{1.638}S_3$
Sb1Bi3-6	1:3	800	3	0.319	1.672	3.009	0.160/0.840	$Sb_{0.320}Bi_{1.680}S_3$

TABLE 3. Atomic coordinates and equivalent isotropic parameters (Å²) for stibnite (Sb_2S_3), bismuthinite (Bi_2S_3), and synthetic $(Sb,Bi)_2S_3$

Atom	x	y	z	B_{eq}	Occ.(Sb/Bi)
$Sb_{2.000}S_3$(1)					
Sb1	0.47063(4)	0.25	0.32602(3)	1.22(1)	0.5000/0.0000
Sb2	0.35061(4)	0.75	0.03603(4)	1.53(1)	0.5000/0.0000
S1	0.2922(1)	0.25	0.1918(1)	1.16(3)	
S2	0.5496(1)	0.75	0.1231(1)	1.20(3)	
S3	0.3748(1)	0.75	0.4388(1)	1.24(3)	
$Sb_{2.000}S_3$(2)					
Sb1	0.47061(3)	0.25	0.32595(3)	1.449(8)	0.5000/0.0000
Sb2	0.35059(3)	0.75	0.03602(3)	1.755(8)	0.5000/0.0000
S1	0.29214(9)	0.25	0.19181(9)	1.39(2)	
S2	0.5498(1)	0.75	0.1230(1)	1.46(2)	
S3	0.3751(1)	0.75	0.4389(1)	1.45(2)	
$Sb_{2.000}S_3$(3)					
Sb1	0.47058(5)	0.25	0.32599(5)	1.53(1)	0.5000/0.0000
Sb2	0.35060(5)	0.75	0.03600(6)	1.82(1)	0.5000/0.0000
S1	0.2918(2)	0.25	0.1919(2)	1.49(4)	
S2	0.5496(2)	0.75	0.1229(2)	1.56(4)	
S3	0.3754(2)	0.75	0.4389(2)	1.50(4)	
$Sb_{2.000}S_3$(4)					
Sb1	0.47065(2)	0.25	0.32599(2)	1.279(7)	0.5000/0.0000
Sb2	0.35054(2)	0.75	0.03603(2)	1.587(7)	0.5000/0.0000
S1	0.29215(9)	0.25	0.19193(8)	1.27(2)	
S2	0.54969(8)	0.75	0.12291(9)	1.27(2)	
S3	0.37495(9)	0.75	0.43873(8)	1.28(2)	
$Sb_{1.935}Bi_{0.065}S_3$					
M1	0.47149(1)	0.25	0.32601(1)	1.406(8)	0.482(1)/0.018(1)
M2	0.34992(1)	0.75	0.03608(1)	1.728(9)	0.486(1)/0.014(1)
S1	0.2918(1)	0.25	0.1919(1)	1.35(2)	
S2	0.5496(1)	0.75	0.1231(1)	1.32(2)	
S3	0.3751(1)	0.75	0.4388(1)	1.32(2)	
$Sb_{1.637}Bi_{0.363}S_3$					
M1	0.47560(1)	0.25	0.32610(1)	2.11(2)	0.398(3)/0.102(3)
M2	0.34720(1)	0.75	0.03520(1)	2.30(2)	0.420(3)/0.080(3)
S1	0.2898(4)	0.25	0.1925 (4)	2.07(9)	
S2	0.5491(4)	0.75	0.1252(4)	2.28(9)	
S3	0.3756(4)	0.75	0.4396(5)	2.33(9)	
$Sb_{1.483}Bi_{0.517}S_3$					
M1	0.47440(1)	0.25	0.32590(1)	2.48(3)	0.349(4)/0.151(4)
M2	0.34790(1)	0.75	0.03550(1)	2.55(3)	0.393(4)/0.107(4)
S1	0.2913(4)	0.25	0.1924(5)	1.9(1)	
S2	0.5492(4)	0.75	0.1250(5)	1.7(1)	
S3	0.3754(5)	0.75	0.4395(5)	2.0(1)	
$Sb_{1.463}Bi_{0.537}S_3$					
M1	0.47430(1)	0.25	0.32630(1)	1.85(2)	0.351(3)/0.149(3)
M2	0.34820(1)	0.75	0.03520(1)	2.04(2)	0.381(3)/0.119(3)
S1	0.2908(3)	0.25	0.1926(3)	1.40(6)	
S2	0.5492(3)	0.75	0.1237(3)	1.41(6)	
S3	0.3755(3)	0.75	0.4395(3)	1.44(6)	

TABLE 3.—*continued*

Atom	x	y	z	B_{eq}	Occ.(Sb/Bi)
$Sb_{1.426}Bi_{0.574}S_3$					
M1	0.47530(1)	0.25	0.32590(1)	2.00(2)	0.342(3)/0.158(3)
M2	0.34720(1)	0.75	0.03490(1)	2.16(2)	0.372(3)/0.128(3)
S1	0.2907(3)	0.25	0.1924(3)	1.75(7)	
S2	0.5493(3)	0.75	0.1243(3)	1.85(7)	
S3	0.3754(3)	0.75	0.4395(3)	1.89(7)	
$Sb_{0.910}Bi_{1.090}S_3$					
M1	0.47868(1)	0.25	0.32581(1)	1.76(2)	0.213(5)/0.287(5)
M2	0.34476(1)	0.75	0.03390(1)	1.83(3)	0.242(5)/0.258(5)
S1	0.2872(4)	0.25	0.1929(4)	1.35(9)	
S2	0.5491(4)	0.75	0.1276(5)	1.35(9)	
S3	0.3746(5)	0.75	0.4410(5)	1.51(9)	
$Sb_{0.387}Bi_{1.613}S_3$					
M1	0.48158(1)	0.25	0.32569(1)	1.71(2)	0.089(4)/0.411(4)
M2	0.34232(1)	0.75	0.03411(1)	1.82(3)	0.105(4)/0.395(4)
S1	0.2850(5)	0.25	0.1939(4)	1.3(1)	
S2	0.5495(5)	0.75	0.1287(5)	1.37(9)	
S3	0.3756(5)	0.75	0.4415(5)	1.6(1)	
$Sb_{0.362}Bi_{1.638}S_3$					
M1	0.48127(1)	0.25	0.32580(1)	1.38(1)	0.083(3)/0.417(3)
M2	0.34257(1)	0.75	0.03429(1)	1.49(1)	0.098(3)/0.402(3)
S1	0.2862(3)	0.25	0.1931(3)	0.96(6)	
S2	0.5494(3)	0.75	0.1275(3)	1.04(6)	
S3	0.3762(3)	0.75	0.4411(3)	1.14(6)	
$Sb_{0.320}Bi_{1.680}S_3$					
M1	0.48165(1)	0.25	0.32575(1)	1.310(8)	0.072(1)/0.428(1)
M2	0.34226(1)	0.75	0.03421(1)	1.396(8)	0.088(1)/0.412(1)
S1	0.2850(2)	0.25	0.1937(1)	0.96(3)	
S2	0.5496(2)	0.75	0.1279(2)	0.89(3)	
S3	0.3759(2)	0.75	0.4414(2)	1.08(3)	
$Bi_{2.000}S_3$(1)					
Bi1	0.48339(7)	0.25	0.32581(8)	1.46(2)	0.0000/0.5000
Bi2	0.34069(7)	0.75	0.03429(7)	1.58(2)	0.0000/0.5000
S1	0.2854(5)	0.25	0.1941(4)	1.12(9)	
S2	0.5500(5)	0.75	0.1284(5)	1.32(9)	
S3	0.3756(5)	0.75	0.4423(5)	1.27(9)	
$Bi_{2.000}S_3$(2)					
Bi1	0.4835(1)	0.25	0.3257(1)	1.47(2)	0.0000/0.5000
Bi2	0.3407(1)	0.75	0.0339(1)	1.50(2)	0.0000/0.5000
S1	0.2835(6)	0.25	0.1943(6)	1.1(1)	
S2	0.5495(6)	0.75	0.1286(7)	1.2(1)	
S3	0.3767(6)	0.75	0.4414(6)	1.0(1)	
$Bi_{2.000}S_3$(3)					
Bi1	0.4833(1)	0.25	0.3256(1)	1.30(2)	0.0000/0.5000
Bi2	0.3408(1)	0.75	0.0341(1)	1.42(2)	0.0000/0.5000
S1	0.2829(6)	0.25	0.1920(6)	0.9(1)	
S2	0.5492(6)	0.75	0.1287(7)	0.9(1)	
S3	0.3752(6)	0.75	0.4425(6)	0.8(1)	

al. (2002), the M1 site in stibnite can be coordinated to (3 + 4) ligand atoms of sulfur. The three short M1-S bond lengths (M1-S1, M1-S3 × 2) elongate linearly with increasing Bi concentration up to the end-member (Fig. 3). The M1–S1 interatomic distance increases by 8.3% from 2.514 Å in stibnite to 2.723 Å in bismuthinite (Table 5). On the other hand, the four long M1-S bond distances (M1-S2 × 2, M1-S3′, M1-S1′) decrease from stibnite to bismuthinite (Table 5). In particular, the M1–S3′ distance decreases linearly by 3.8% and the M1-S1′ distance by 6.5% (Table 5). These decreasing bond distances between shortest and longest bonds in the coordination polyhedra of Sb^{3+} and Bi^{3+} were substantiated by the views of Makovicky (1992). According to the Valence Shell Electron Pair Repulsion (VSEPR) theory (McKenna and McKenna 1984), lone-pair electrons in the M1 coordination environment can be considered to exist on the same side as S2, S1′, and S3′ atoms in the solid solution. Taking into account the coordination environment enclosing lone-pair

TABLE 4. Anisotropic displacement parameters (Å²) for stibnite (Sb_2S_3), bismuthinite (Bi_2S_3), and synthetic $(Sb,Bi)_2S_3$

Atom	U_{11}	U_{22}	U_{33}	U_{12}	U_{13}	U_{23}
$Sb_{2.000}S_3$(1)						
Sb1	0.0193(3)	0.0106(3)	0.0164(3)	0.0000	–0.0017(1)	0.0000
Sb2	0.0181(3)	0.0169(3)	0.0230(3)	0.0000	0.0044(1)	0.0000
S1	0.0158(7)	0.0146(7)	0.0135(6)	0.0000	0.0009(5)	0.0000
S2	0.0165(7)	0.0126(8)	0.0166(7)	0.0000	0.0016(5)	0.0000
S3	0.0219(7)	0.0114(7)	0.0137(6)	0.0000	–0.0028(5)	0.0000
$Sb_{2.000}S_3$(2)						
Sb1	0.0216(2)	0.0147(2)	0.0187(2)	0.0000	0.0017(1)	0.0000
Sb2	0.0210(2)	0.0208(2)	0.0249(2)	0.0000	–0.0043(1)	0.0000
S1	0.0204(5)	0.0169(5)	0.0155(5)	0.0000	–0.0011(4)	0.0000
S2	0.0209(5)	0.0158(6)	0.0186(5)	0.0000	–0.0023(4)	0.0000
S3	0.0228(5)	0.0161(6)	0.0162(5)	0.0000	0.0031(4)	0.0000
$Sb_{2.000}S_3$(3)						
Sb1	0.0230(4)	0.0173(4)	0.0179(4)	0.0000	0.0018(2)	0.0000
Sb2	0.0226(4)	0.0230(4)	0.0236(4)	0.0000	–0.0044(2)	0.0000
S1	0.025(1)	0.018(1)	0.0137(9)	0.0000	–0.0014(8)	0.0000
S2	0.024(1)	0.017(1)	0.0184(9)	0.0000	–0.0013(8)	0.0000
S3	0.025(1)	0.017(1)	0.0146(9)	0.0000	0.0022(7)	0.0000
$Sb_{2.000}S_3$(4)						
Sb1	0.0181(2)	0.0133(2)	0.0172(2)	0.0000	0.00181(9)	0.0000
Sb2	0.0166(2)	0.0197(2)	0.0240(2)	0.0000	–0.00447(9)	0.0000
S1	0.0168(4)	0.0172(5)	0.0144(4)	0.0000	–0.0011(3)	0.0000
S2	0.0157(4)	0.0156(5)	0.0169(4)	0.0000	–0.0015(3)	0.0000
S3	0.0200(4)	0.0144(5)	0.0143(4)	0.0000	0.0024(3)	0.0000
$Sb_{1.935}Bi_{0.065}S_3$						
M1	0.0207(2)	0.0148(2)	0.0180(2)	0.0000	–0.0017(1)	0.0000
M2	0.0190(2)	0.0216(2)	0.0251(2)	0.0000	0.0043(1)	0.0000
S1	0.0193(5)	0.0173(6)	0.0148(5)	0.0000	0.0010(4)	0.0000
S2	0.0167(5)	0.0159(6)	0.0176(5)	0.0000	0.0018(4)	0.0000
S3	0.0200(5)	0.0156(6)	0.0147(5)	0.0000	–0.0018(4)	0.0000
$Sb_{1.637}Bi_{0.363}S_3$						
M1	0.0244(5)	0.0269(6)	0.0288(6)	0.0000	0.0012(5)	0.0000
M2	0.0188(6)	0.0322(8)	0.0365(8)	0.0000	–0.0021(5)	0.0000
S1	0.020(2)	0.027(2)	0.031(2)	0.0000	–0.001(2)	0.0000
S2	0.020(2)	0.037(3)	0.029(2)	0.0000	–0.000(2)	0.0000
S3	0.023(2)	0.035(3)	0.031(2)	0.0000	0.002(2)	0.0000
$Sb_{1.483}Bi_{0.517}S_3$						
M1	0.0270(7)	0.0283(8)	0.0390(9)	0.0000	0.0020(6)	0.0000
M2	0.0202(7)	0.0325(9)	0.044(1)	0.0000	–0.0028(6)	0.0000
S1	0.013(2)	0.026(3)	0.033(3)	0.0000	–0.001(2)	0.0000
S2	0.013(2)	0.023(3)	0.028(3)	0.0000	–0.003(2)	0.0000
S3	0.020(2)	0.027(3)	0.031(3)	0.0000	0.002(2)	0.0000
$Sb_{1.463}Bi_{0.537}S_3$						
M1	0.0262(5)	0.0210(5)	0.0232(5)	0.0000	0.0016(3)	0.0000
M2	0.0203(5)	0.0259(6)	0.0312(6)	0.0000	–0.0028(4)	0.0000
S1	0.018(2)	0.018(2)	0.017(1)	0.0000	–0.000(1)	0.0000
S2	0.017(1)	0.017(2)	0.019(2)	0.0000	–0.004(1)	0.0000
S3	0.020(2)	0.019(2)	0.015(1)	0.0000	0.002(1)	0.0000
$Sb_{1.426}Bi_{0.574}S_3$						
M1	0.0345(5)	0.0196(4)	0.0219(4)	0.0000	–0.0022(3)	0.0000
M2	0.0289(5)	0.0244(5)	0.0286(5)	0.0000	0.0027(4)	0.0000
S1	0.028(2)	0.021(2)	0.017(2)	0.0000	0.004(1)	0.0000
S2	0.027(2)	0.023(2)	0.021(2)	0.0000	0.002(1)	0.0000
S3	0.028(2)	0.025(2)	0.019(2)	0.0000	–0.005(1)	0.0000
$Sb_{0.910}Bi_{1.090}S_3$						
M1	0.0289(6)	0.0189(6)	0.0189(6)	0.0000	0.0019(5)	0.0000
M2	0.0213(6)	0.0229(7)	0.0253(7)	0.0000	–0.0022(4)	0.0000
S1	0.018(2)	0.019(2)	0.014(2)	0.0000	–0.005(2)	0.0000
S2	0.016(2)	0.020(2)	0.015(2)	0.0000	0.001(2)	0.0000
S3	0.022(3)	0.019(3)	0.017(2)	0.0000	0.008(2)	0.0000
$Sb_{0.387}Bi_{1.613}S_3$						
M1	0.0307(6)	0.0154(5)	0.0190(5)	0.0000	0.0023(4)	0.0000
M2	0.0256(5)	0.0199(5)	0.0236(5)	0.0000	–0.0011(4)	0.0000
S1	0.024(3)	0.015(2)	0.011(2)	0.0000	–0.003(2)	0.0000
S2	0.021(3)	0.016(3)	0.015(2)	0.0000	–0.003(2)	0.0000
S3	0.028(3)	0.020(3)	0.014(2)	0.0000	0.001(2)	0.0000
$Sb_{0.362}Bi_{1.638}S_3$						
M1	0.0184(4)	0.0145(3)	0.0194(4)	0.0000	0.0029(2)	0.0000
M2	0.0131(3)	0.0194(4)	0.0240(4)	0.0000	–0.0017(2)	0.0000
S1	0.007(1)	0.016(2)	0.014(1)	0.0000	0.001(1)	0.0000
S2	0.011(1)	0.016(2)	0.013(1)	0.0000	–0.000(1)	0.0000
S3	0.011(1)	0.019(2)	0.014(1)	0.0000	0.002(1)	0.0000
$Sb_{0.320}Bi_{1.680}S_3$						
M1	0.0198(2)	0.0136(2)	0.0163(2)	0.0000	0.0027(1)	0.0000
M2	0.0146(2)	0.0178(2)	0.0206(2)	0.0000	–0.0014(1)	0.0000
S1	0.0122(7)	0.0158(8)	0.0086(8)	0.0000	–0.0018(7)	0.0000
S2	0.0130(7)	0.0123(9)	0.0085(7)	0.0000	0.0015(7)	0.0000
S3	0.0143(8)	0.0161(8)	0.0107(7)	0.0000	0.0020(7)	0.0000
$Bi_{2.000}S_3$(1)						
Bi1	0.0215(5)	0.0164(5)	0.0175(5)	0.0000	–0.0034(3)	0.0000
Bi2	0.0184(5)	0.0213(5)	0.0204(5)	0.0000	0.0012(3)	0.0000
S1	0.016(2)	0.013(2)	0.013(2)	0.0000	–0.002(2)	0.0000
S2	0.018(2)	0.019(3)	0.014(2)	0.0000	0.001(2)	0.0000
S3	0.017(2)	0.018(2)	0.013(2)	0.0000	–0.002(2)	0.0000
$Bi_{2.000}S_3$(2)						
Bi1	0.0199(6)	0.0150(6)	0.0208(6)	0.0000	0.0040(5)	0.0000
Bi2	0.0158(5)	0.0192(7)	0.0221(6)	0.0000	–0.0018(4)	0.0000
S1	0.013(3)	0.016(4)	0.013(3)	0.0000	–0.004(3)	0.0000
S2	0.017(3)	0.015(3)	0.014(3)	0.0000	0.003(3)	0.0000
S3	0.012(3)	0.016(4)	0.009(3)	0.0000	0.003(3)	0.0000
$Bi_{2.000}S_3$(3)						
Bi1	0.0216(6)	0.0107(5)	0.0172(6)	0.0000	–0.0023(5)	0.0000
Bi2	0.0192(6)	0.0150(6)	0.0199(6)	0.0000	0.0012(5)	0.0000
S1	0.014(3)	0.016(3)	0.003(3)	0.0000	0.004(3)	0.0000
S2	0.010(3)	0.012(3)	0.014(3)	0.0000	–0.003(3)	0.0000
S3	0.011(3)	0.014(4)	0.005(3)	0.0000	–0.001(3)	0.0000

electrons, the three elongating bonds exist on the side opposite to the lone-pair electrons, whereas the four shrinking bonds are in the direction of the lone-pair electrons. A more pronounced change was observed in the S1′-M1-S3′ interatomic angle (Fig. 4). The angle shows the greatest change by increasing from 59.67° in stibnite to 62.4° in bismuthinite; an increase of 4.6%. Moreover, a similar change was also observed in the S2-M1-S3′ angle (Fig. 4), which increases by 2.0% from 116.87° in stibnite to 119.2° in bismuthinite. The other interatomic angles within the M1 site decrease with increasing Bi concentration (Fig. 4). These changes in both interatomic distances and angles can be regarded as the result of transformation of stereochemical activity from Sb $5s^2$ lone-pair electrons to Bi $6s^2$ lone-pair electrons. These lone-pair electrons are known to cause a non-spherical charge distribution around their cations (e.g., Downs 1993). This modification of the structure suggests that the orbital of the lone-pair electrons actually changes from a highly elongated ellipsoid to a more spherical one (Fig. 5). It is readily inferred that expansions of short M1-S bonds (M1-S1, M1-S3 × 2) existing on the opposite side of lone-pair electrons are attributable to an increase of ionic radii from Sb^{3+} to Bi^{3+}, which is nearly 40% (Shannon 1976).

The M2 site

The M2 site in stibnite can be regarded as being in a (5 + 2) sulfur coordination (Skowron and Brown 1994; Kyono et al. 2002). Skowron and Brown (1994) suggested that the two secondary bonds to the M2 site are responsible for cohesion and packing in stibnite. These two secondary M2-S3′ bonds shrink slightly with increasing Bi concentration (Fig. 6). On the other hand, the five shorter bonds (M2-S2, M2-S1 × 2, M2-S2′ × 2) arranged at the vertices of a square pyramid elongate significantly from stibnite to bismuthinite (Fig. 6). The M2-S2 and M2-S2′ bond lengths in particular increase by 6.0% and 4.7%, respectively (Table 5). Increases of the five bond lengths are caused mainly by the distinct increase of ionic radii from Sb^{3+} to Bi^{3+}. The largest changes in the $M2S_7$ coordination polyhedron were observed for the S3′-M2-S3″ angle (Fig. 7). The lone-pair electrons below the square pyramid are interposed between the long secondary bonds (Skowron and Brown 1994). This S3′-M2-S3″ interatomic

TABLE 5. Selected interatomic distances (Å) for stibnite (Sb_2S_3), bismuthinite (Bi_2S_3), and synthetic $(Sb,Bi)_2S_3$

Chemical composition		$Sb_{2.000}S_3$(1)	$Sb_{2.000}S_3$(2)	$Sb_{2.000}S_3$(3)	$Sb_{2.000}S_3$(4)	$Sb_{1.935}Bi_{0.065}S_3$	$Sb_{1.637}Bi_{0.363}S_3$	$Sb_{1.483}Bi_{0.517}S_3$	$Sb_{1.463}Bi_{0.537}S_3$
M1	S1	2.514(2)	2.518(1)	2.515(2)	2.520(1)	2.530(1)	2.572(4)	2.556(5)	2.558(3)
	S3 × 2[a]	2.537(1)	2.541(1)	2.531(1)	2.540(1)	2.546(1)	2.574(3)	2.577(4)	2.569(2)
	S2 × 2[a]	3.106(1)	3.110(1)	3.102(2)	3.111(1)	3.108(1)	3.077(4)	3.092(4)	3.098(3)
	S3[b]	3.164(2)	3.164(1)	3.155(2)	3.169(1)	3.158(1)	3.107(5)	3.132(6)	3.122(4)
	S1[c]	3.633(2)	3.642(1)	3.630(2)	3.645(1)	3.628(1)	3.548(4)	3.593(5)	3.586(3)
M2	S2	2.448(2)	2.456(1)	2.448(2)	2.456(1)	2.461(1)	2.488(4)	2.489(5)	2.479(3)
	S1 × 2[d]	2.676(1)	2.679(1)	2.672(2)	2.679(1)	2.680(1)	2.693(3)	2.696(4)	2.695(2)
	S2 × 2[ef]	2.850(1)	2.853(1)	2.844(2)	2.852(1)	2.859(1)	2.885(4)	2.891(4)	2.873(3)
	S3 × 2[gh]	3.365(1)	3.375(1)	3.367(2)	3.374(1)	3.371(1)	3.346(4)	3.363(4)	3.360(3)

Chemical composition		$Sb_{1.426}Bi_{0.574}S_3$	$Sb_{0.910}Bi_{1.090}S_3$	$Sb_{0.387}Bi_{1.613}S_3$	$Sb_{0.362}Bi_{1.638}S_3$	$Sb_{0.320}Bi_{1.680}S_3$	$Bi_{2.000}S_3$(1)	$Bi_{2.000}S_3$(2)	$Bi_{2.000}S_3$(3)
M1	S1	2.572(3)	2.620(5)	2.672(5)	2.658(3)	2.669(2)	2.681(5)	2.704(7)	2.723(6)
	S3 × 2[a]	2.585(2)	2.614(3)	2.652(4)	2.642(2)	2.647(1)	2.669(3)	2.670(5)	2.683(5)
	S2 × 2[a]	3.099(3)	3.059(4)	3.060(4)	3.068(3)	3.062(1)	3.063(4)	3.069(6)	3.065(6)
	S3[b]	3.130(4)	3.090(6)	3.066(6)	3.064(4)	3.059(2)	3.043(5)	3.052(7)	3.052(7)
	S1[c]	3.575(4)	3.478(5)	3.447(6)	3.456(3)	3.440(2)	3.425(5)	3.411(7)	3.407(7)
M2	S2	2.497(4)	2.528(5)	2.576(5)	2.561(4)	2.569(2)	2.592(6)	2.595(7)	2.593(7)
	S1 × 2[d]	2.704(2)	2.719(4)	2.744(3)	2.732(2)	2.739(1)	2.743(3)	2.763(5)	2.745(5)
	S2 × 2[ef]	2.889(3)	2.915(4)	2.955(4)	2.945(3)	2.947(1)	2.962(4)	2.974(5)	2.977(5)
	S3 × 2[gh]	3.358(3)	3.313(4)	3.330(5)	3.333(3)	3.329(1)	3.315(4)	3.339(6)	3.323(6)

Notes: Symmetry codes: (a) x, 1 + y, z; (b) 1 – x, 1/2 + y, 1 – z; (c) 1/2 + x, 1/2 – y, 1/2 – z; (d) x, –1 + y, z; (e) 1 – x, –1/2 + y, –z; (f) 1 – x, 1/2 + y, –z; (g) 1/2 – x, –y, –1/2 + z; (h) 1/2 – x, –1 – y, –1/2 + z.

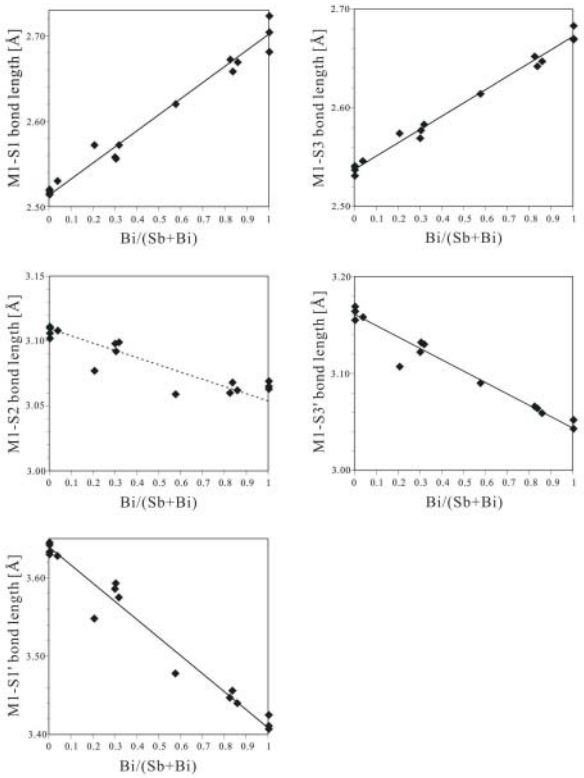

FIGURE 3. Selected M1-S bond lengths for the synthetic stibnite-bismuthinite $(Sb,Bi)_2S_3$ solid solution series as determined from single crystal structure refinements. Explanation of the straight lines is given in Figure 2.

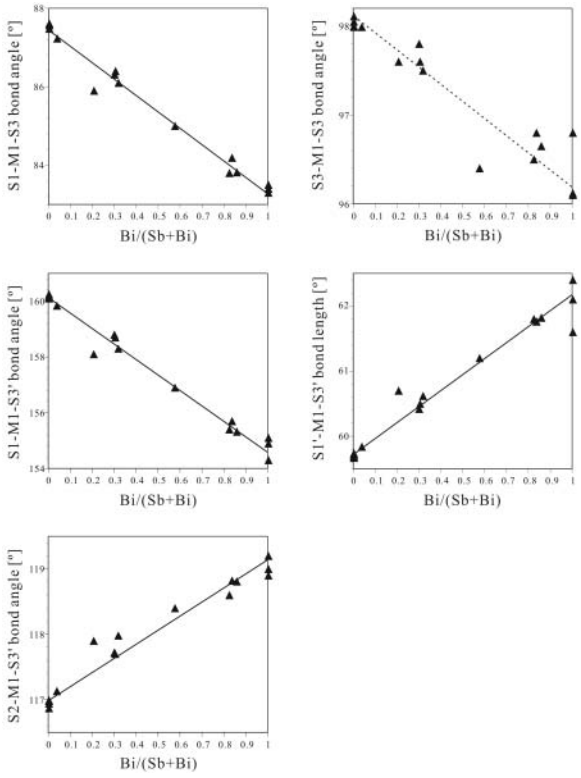

FIGURE 4. Selected M1-S bond angles for the synthetic stibnite-bismuthinite $(Sb,Bi)_2S_3$ solid solution series as determined from single-crystal structure refinements. Explanation of the straight lines is given in Figure 2.

angle below the square pyramid shows the greatest increase, from 69.16° in stibnite to 73.8° in bismuthinite. Therefore, substitution of Bi^{3+} for Sb^{3+} gives rise to an increase of the interatomic angle interposing lone-pair electrons, which corresponds well with changes of stereochemical activity at the M1 site (Fig. 4). Interatomic angles between the axial bond and each basal bond in a square pyramid apparently decrease (Fig. 7).

Variations in $M1S_7$ and $M2S_7$ polyhedra

The M1 and M2 coordination polyhedra that form the basic building block are connected by S1 sulfur atoms. Increasing Bi concentration produces a linear decrease in the M1-S1-M2 interatomic angle (Fig. 8) of 2.4% from 101.21° to 98.8°. The M2 coordination polyhedra are interconnected by S2′ sulfur atoms; Fig. 8 shows that the M2-S2′-M2 interatomic angle increases

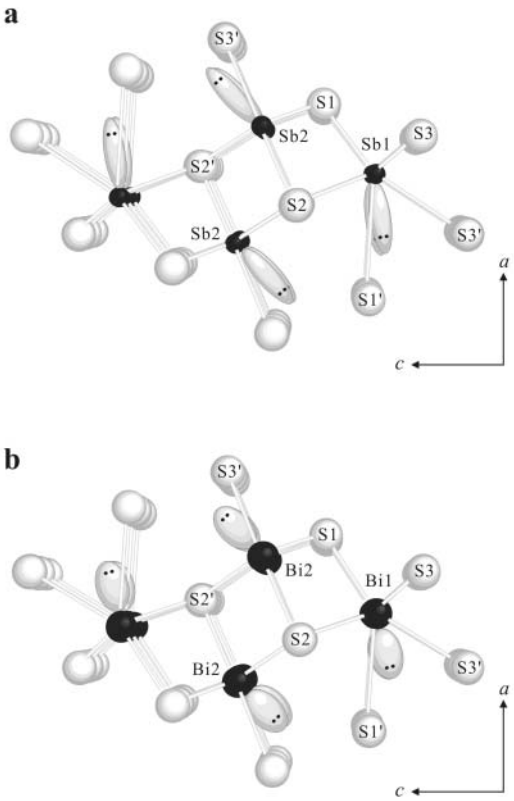

FIGURE 5. Connection between $M1S_7$ and $M2S_7$ polyhedra in (**a**) stibnite and (**b**) bismuthinite. The stereoactive lone-pair electrons are shown schematically.

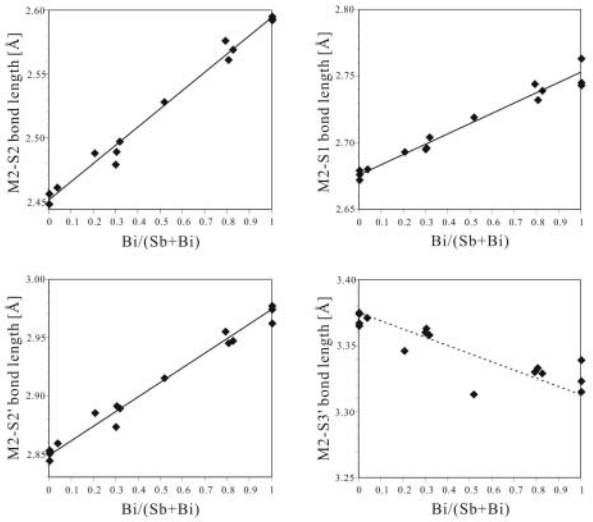

FIGURE 6. Selected M2-S bond lengths for the synthetic stibnite-bismuthinite $(Sb,Bi)_2S_3$ solid solution series as determined from single crystal structure refinements. Explanation of the straight lines is given in Figure 2.

by 1.2% from 96.44° in stibnite to 97.6° in bismuthinite; this contrasts with the variation of the M1-S1-M2 angle. Concerning deformation of the coordination environment enclosing the lone-pair electrons, linear decreases of bond lengths close to the direction of the lone-pair electrons are found to be associated with both the M1 and M2 polyhedra. Bond lengths on the side opposite to the lone-pair electrons, on the contrary, become longer for both the M1 and M2 polyhedra. Noteworthy increases of interatomic angles interposing lone-pair electrons result from this connection. According to the VSEPR theory (McKenna and McKenna 1984), these variations in interatomic angles indicate that transformation of stereochemical activity engenders geometric deformation of the basic building block.

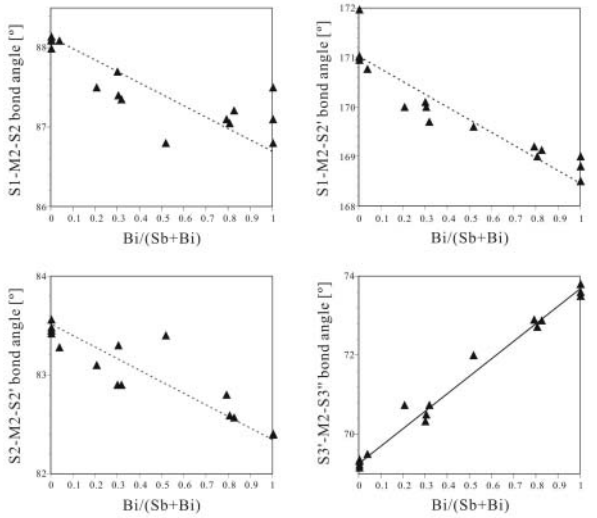

FIGURE 7. Selected M2-S bond angles for the synthetic stibnite-bismuthinite $(Sb,Bi)_2S_3$ solid solution series as determined from single-crystal structure refinements. Explanation of the straight lines is given in Figure 2.

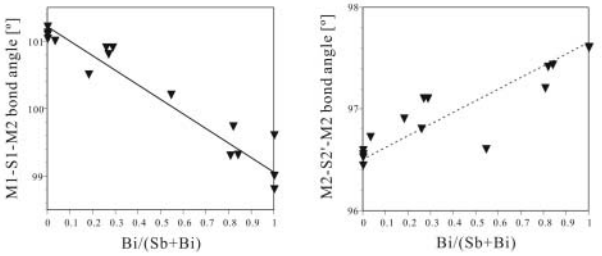

FIGURE 8. Variations of polyhedral bridging angles for the synthetic stibnite-bismuthinite $(Sb,Bi)_2S_3$ solid solution series as determined from single-crystal structure refinements. Explanation of the straight lines is given in Figure 2.

Expansion of the basic building block affects the *b* lattice parameter because the basic building block in the $(Sb,Bi)_2S_3$ solid solution is composed of infinite $[M_2S_4]$ ribbons running parallel to **b**. The *b* lattice parameter increases linearly with increasing Bi content (Fig. 2) because the basic building block along **b** is made up of continuously increasing M-S bonds. On the other hand, increasing the Bi concentration induces expansion of the basic building block, but the higher the concentration of Bi, the narrower the intervals between basic building blocks. That is to say, the M-S bonds affecting *a* and *c* lattice parameters can compensate for decreases of secondary bond distances with expansion of the basic building block. For this reason, changes of both *a* and *c* lattice parameters are smaller than that of the *b* lattice parameter.

Polyhedral variations influenced by stereochemical activity

Polyhedral parameters used are defined in Balić-Žunić and Vickovic (1996) and Makovicky and Balić-Žunić (1998). Table 6 lists the polyhedral parameters calculated with the IVTON program (Balić-Žunić and Vickovic 1996). Although there are two kinds of anisotropic geometrical changes of M1 and M2 polyhedra in the solid solution, these polyhedral volumes expand while retaining their sphericities (Fig. 9). Because volumes of $M1S_7$ coordination polyhedra are always larger than those of $M2S_7$ coordination polyhedra in the $(Sb,Bi)_2S_3$ solid solution (Table 6), Bi^{3+} tends to occupy the M1 site in preference to the M2 site (Table 3). Partial ordering of Bi cation at the M1 and M2 sites is consistent with slight positive deviation from Vegard's law in the *b* cell parameters. However, with increasing Bi concentration, Bi^{3+} site occupancy of M2 increases considerably compared to that of M1 (Table 3). Indeed, we observed expansion of the M2 polyhedron: it nearly achieved the volume of the M1 polyhedron (Table 6 and Fig. 9). Consequently, the M1 polyhedron volume increases by 3.7% with increasing Bi concentration, but the volume of the M2 polyhedron increases continuously by 8.2% (Fig. 9). It is noteworthy that expansibility of the M2 polyhedron is 2.2 times as large as that of the M1 polyhedron in this solid solution. The most pronounced geometrical change in the solid solution was the change in the distance between the centroid and the central atom (cation eccentricity) for the M1 polyhedron (Fig. 10). With increasing Bi concentration, this distance decreases drastically by 35.2% from 0.660 Å to 0.428 Å (Table 6). The distance for the M2 polyhedron also decreases remark-

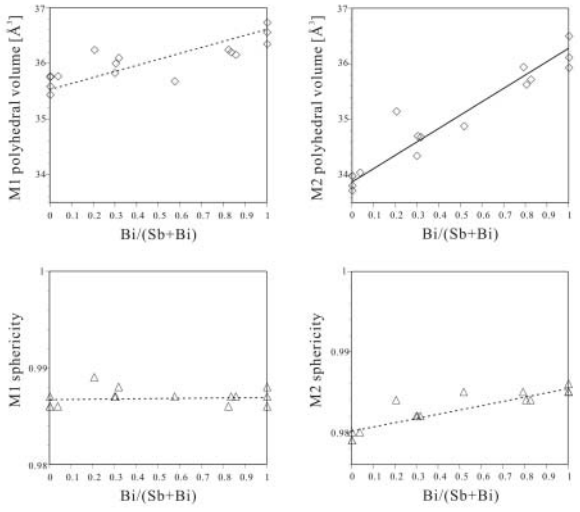

FIGURE 9. Variations of polyhedral distortion parameters for the synthetic stibnite-bismuthinite $(Sb,Bi)_2S_3$ solid solution series as calculated by the IVTON program (Balić-Žunić and Vickovic 1996). Explanation of the straight lines is given in Figure 2.

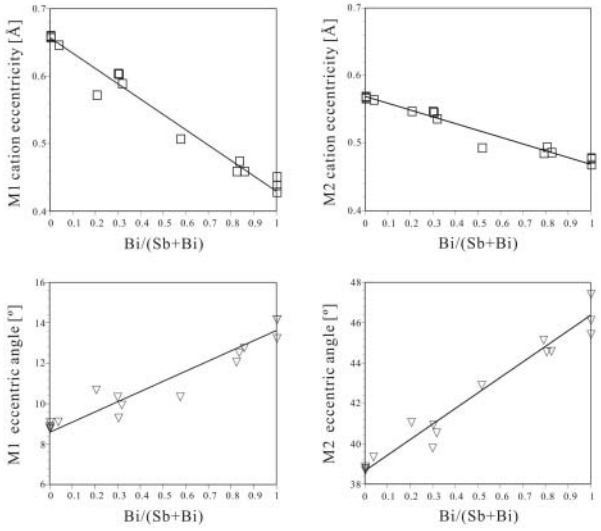

FIGURE 10. Variations of polyhedral eccentric parameters for the synthetic stibnite-bismuthinite $(Sb,Bi)_2S_3$ solid solution series as calculated by the IVTON program (Balić-Žunić and Vickovic 1996). Explanation of the straight lines is given in Figure 2.

TABLE 6. Polyhedral distortion parameters calculated with the IVTON program (Balić-Žunić and Vickovic 1996)

Chemical composition	$Sb_{2.000}S_3$(1)	$Sb_{2.000}S_3$(2)	$Sb_{2.000}S_3$(3)	$Sb_{2.000}S_3$(4)	$Sb_{1.935}Bi_{0.065}S_3$	$Sb_{1.637}Bi_{0.363}S_3$	$Sb_{1.483}Bi_{0.517}S_3$	$Sb_{1.463}Bi_{0.537}S_3$
V_{M1} (Å³)	35.580	35.751	35.430	35.760	35.763	36.325	35.993	35.820
r_{M1} (Å)	2.943	2.947	2.938	2.948	2.947	2.952	2.949	2.945
s_{M1}	0.987	0.986	0.986	0.986	0.986	0.989	0.987	0.987
Δ_{M1} (Å)	0.657	0.659	0.657	0.660	0.646	0.572	0.603	0.604
α1(°)	8.75	8.87	9.05	8.79	9.09	10.67	9.28	10.31
V_{M2} (Å³)	33.804	33.978	33.718	33.981	34.042	35.140	34.696	34.341
r_{M2} (Å)	2.899	2.905	2.897	2.905	2.907	2.941	2.925	2.916
s_{M2}	0.980	0.979	0.979	0.979	0.980	0.984	0.982	0.982
Δ_{M2} (Å)	0.566	0.569	0.569	0.568	0.564	0.547	0.545	0.547
α2(°)	38.85	38.75	38.66	38.76	39.33	41.04	40.92	39.77

Chemical composition	$Sb_{1.426}Bi_{0.574}S_3$	$Sb_{0.910}Bi_{1.090}S_3$	$Sb_{0.387}Bi_{1.613}S_3$	$Sb_{0.362}Bi_{1.638}S_3$	$Sb_{0.320}Bi_{1.680}S_3$	$Bi_{2.000}S_3$(1)	$Bi_{2.000}S_3$(2)	$Bi_{2.000}S_3$(3)
V_{M1} (Å³)	36.092	35.673	36.238	36.194	36.149	36.342	36.554	36.725
r_{M1} (Å)	2.951	2.935	2.946	2.944	2.943	2.947	2.951	2.955
s_{M1}	0.988	0.987	0.986	0.987	0.987	0.988	0.987	0.986
Δ_{M1} (Å)	0.589	0.507	0.459	0.474	0.459	0.438	0.428	0.451
α1(°)	9.92	10.32	12.04	12.50	12.74	13.21	14.14	14.15
V_{M2} (Å³)	34.678	34.875	35.937	35.622	35.713	35.925	36.494	36.108
r_{M2} (Å)	2.925	2.927	2.958	2.951	2.953	2.958	2.974	2.965
s_{M2}	0.982	0.985	0.985	0.984	0.984	0.985	0.986	0.985
Δ_{M2} (Å)	0.536	0.493	0.485	0.494	0.486	0.468	0.477	0.478
α2(°)	40.52	42.88	45.12	44.53	44.56	46.10	45.40	47.39

Notes: V = polyhedron volume; r = radius of the least-squares sphere fitted to the polyhedron; s = sphericity equals to $(1 - \sigma_r/r)$ where σ_r is standard deviation of r; Δ = distances between the centroid and central atom of the polyhedron (cation eccentricity); α = angles of centroid-central atom to **a** (eccentric angle).

ably by 17.8% (Table 6), but variation in the centroid-central atom distance for the M1 polyhedron is almost twice as large as that associated with the M2 polyhedron. Andersson and Åström (1972) suggested that the degree of stereochemical activity can be expressed by centroid-central atom distance. Therefore, the orbital of the lone-pair electrons decreases greatly for both the M1 and M2 polyhedra from stibnite to bismuthinite. These changes indicate the reduced stereochemical activity from Sb $5s^2$ lone-pair electrons to Bi $6s^2$ lone-pair electrons (Makovicky 1992). The inferred decrease of stereochemical activity is approximately consistent with the view of molecular orbital and crystal orbital calculations (Wheeler and Pavan-Kumar 1992). Furthermore, the angles of the centroid-central atom to **a** constantly increase from stibnite to bismuthinite (Fig. 10). This variation is ascribed to increased repulsion between shrinking M-S bonds and lone-pair electrons. One striking characteristic of $(Sb,Bi)_2S_3$ crystal structures is that geometries of central cation and ligand atoms can be adapted flexibly to the transformation of stereochemical activity from Sb $5s^2$ lone-pair electrons to Bi$6s^2$ lone-pair electrons by altering the centroid-central atom distance.

ACKNOWLEDGMENTS

The authors thank T. Hatta at the Japan International Research Center for Agricultural Sciences for performing the SEM-EDS analysis. We also thank R. Sack and E. Makovicky for their constructive comments and Associate Editor A.F. Gualtieri for improving this manuscript. This study was supported by a Research Fellowship of the Japan Society for Promotion of Science received by the first author.

REFERENCES CITED

Altomare, A., Cascarano, G., Giacovazzo, C., Guagliardi, A., Burla, M.C., Polidori, G., and Camalli, M. (1992) SIR92—a program for automatic solution of structures by direct methods. Journal of Applied Crystallography, 27, 435.

Andersson, S. and Åström, A. (1972) Solid state chemistry. Proceedings of the 5th Material Research Symposium, p. 3–14.

Balić-Žunić, T. and Vickovic, I. (1996) IVTON—program for the calculation of geometrical aspects of crystal structures and some crystal chemical applications. Journal of Applied Crystallography, 29, 305 306.

Bayliss, P. and Nowacki, W. (1972) Refinement of the crystal structure of stibnite, Sb_2S_3. Zeitschrift für Kristallographie, 135, 308–315.

Beurskens, P.T., Admiraal, G., Beurskens, G., Bosman, W.P., de Gelder, R., Israel, R., and Smits, J.M.M. (1999) The DIRDIF-99 program system. Technical report of the crystallography laboratory, University of Nijmegen, The Netherlands.

Downs, A.J. (1993) Chemistry of aluminum, gallium, indium and thallium, 526 p. Blackie Academic and Professional, London.

Ghosal, S. and Sack, R.O. (1999) Bi-Sb energetics in sulfosalts and sulfides. Mineralogical Magazine, 63, 723–733.

Kanishcheva, A.S., Mikhailov, Y.N., and Trippel, A.F. (1981) Refinement of the crystal structure of synthetic bismuthinite. Izvestiya Akademii Nauk SSSR, Neorganicheskie Materialy, 17, 1972–1975.

Kazantsev, S.S., Pushcharovsky, D.Y., Maximov, B.A., Molchanov, N.V., Werner, S., Schneider, J., and Sapozhnikov, A.N. (2002) Phase transitions in solid solution series bismutocolumbite-stibiocolumbite (Bi-Sb)$(Nb_{0.79}Ta_{0.21})O_4$. Zeitschrift für Kristallographie, 217, 542–549.

Kyono, A., Kimata, M., Matsuhisa, M., Miyashita, Y., and Okamoto, K. (2002) Low-temperature crystal structures of stibnite implying orbital overlap of Sb $5s^2$ inert pair electrons. Physics and Chemistry of Minerals, 29, 254–260.

Lueth, V.W., Goodell, P.C., and Pingitore, N.E. Jr. (1990) Encoding the evolution of an ore system in bismuthinite-stibnite composition: Julcani, Peru. Economic Geology, 85, 1462–1472.

Łukaszewicz, K., Stępień-Damm, J., Pietraszko, A., Kajokas, A., and Grigas, J. (1999) Crystal structure, thermal expansion, dielectric permittivity and phase transitions of Bi_2S_3. Polish Journal of Chemistry, 73, 541–546.

Lundegaard, F.F., Miletich, R., Balić-Žunić, T., and Makovicky, E. (2003) Equation of state and crystal structure of Sb_2S_3 between 0 and 10 GPa. Physics and Chemistry of Minerals, 30, 463–468.

Makovicky, E. (1981) The building principles and classification of bismuth-lead sulphosalts and related compounds. Fortschritte der Mineralogie, 59, 137–190.

——— (1992) Crystal chemistry of complex sulfides (sulfosalts) and its chemical application. In E. Parthé, Ed., Modern perspectives in inorganic crystal chemistry, p. 131 161. Kluwer Academic Publishers, Boston.

Makovicky, E. and Balić-Žunić, T. (1998) New measure of distortion for coordination polyhedra. Acta Crystallographica, B54, 766–773.

McKenna, A.G. and McKenna, J.F. (1984) Teaching VSEPR theory: the dilemma of five-coordination. Journal of Chemical Education, 61, 771–773.

Nayak, B.B., Acharya, H.N., Mitra, G.B., and Mathur, B.K. (1983) Structural characterization of $Bi_{2-x}Sb_xS_3$ films prepared by the dip-dry method. Thin Solid Films, 105, 17–24.

Pfitzner, A. and Kurowski, D. (2000) A new modification of $MnSb_2S_4$ crystallizing in the $HgBi_2S_4$ structure type. Zeitschrift für Kristallographie, 215, 373–376.

Shannon, R.D. (1976) Revised effective ionic radii and synthetic studies of interatomic distances in halides and chalcogenides. Acta Crystallographica, A32, 751–768.

Skowron, A. and Brown, I.D. (1994) Crystal chemistry and structures of lead-antimony sulfides. Acta Crystallographica, B50, 524–538.

Springer, G. (1969) Naturally occurring compositions in the solid-solution series Bi_2S_3-Sb_2S_3. Mineralogical Magazine, 37, 294–296.

Springer, G. and Laflamme, J.H.G. (1971) The system Bi_2S_3-Sb_2S_3. Canadian Mineralogist, 10, 847–853.

Toman, K. (1978) Ordering in olivenite-adamite solid solution. Acta Crystallographica, B34, 715–721.

Watkin, D.J., Prout, C.K., Carruthers, J.R., and Betteridge, P.W. (1996) CRYSTALS Issue 10. Chemical crystallography laboratory, Oxford, U.K.

Weinberger, P., Drchal, V., Szunyogh, L., and Fritscher, J. (1994) Electronic and structural properties of Cu-Au alloys. Physical Review B, 49, 13366–13372.

Wheeler, R.A. and Pavan-Kumar, P.N.V. (1992) Stereochemically active or inactive lone-pair electrons in some six-coordinate, group 15 halides. Journal of American Chemical Society, 114, 4776–4784.

MANUSCRIPT RECEIVED MARCH 11, 2003
MANUSCRIPT ACCEPTED DECEMBER 7, 2003
MANUSCRIPT HANDLED BY ALESSANDRO GUALTIERI